Electronic Supplementary Material (ESI) for Physical Chemistry Chemical Physics.

Ultrafast geometrical reorganization of a methane cation upon a sudden ionization: An isotope effect in electronic non equilibrium quantum dynamics

Cayo G. M. Gonçalves,[1] R. D. Levine,[2] F. Remacle[1,2,]*

[1]Theoretical Physical Chemistry, University of Liège, 4000 Liège, Belgium :
[2]The Fritz Haber Research Center for Molecular Dynamics, The Hebrew University of Jerusalem, 91904 Jerusalem, Israel

* Corresponding Author : fremacle@uliege.be

Electronic Supplementary Information

Contents

Computational Methods

1. Definition of the coordinates of the grid

CH_4^+ possesses 9 internal coordinates. They are all involved in the configurational distortions leading to the C_{2v} and D_{2d} minima on the ground state of the cation and in the non adiabatic coupling seams between the three lowest excited states. In order to capture the main features of the early time non adiabatic quantum dynamics, we define a grid with two coordinates, q_1 and q_2, that are linear combinations of 15 Cartesian displacements $\Delta_{i\alpha}$:

$$q_1 = \sum_{i=1}^{5} \sum_{\alpha=1}^{3} a_{i\alpha}\Delta_{i\alpha} \quad (1)$$

$$q_2 = \sum_{i=1}^{5} \sum_{\alpha=1}^{3} b_{i\alpha}\Delta_{i\alpha} \quad (2)$$

with α = 1, 2,3 for the three Cartesian displacements $\Delta_{i\alpha}$ on each atom.

Table S1: Normalized Cartesian displacements defining the two coordinates q_1 and q_2

	Δx_C	Δy_C	Δz_C	Δx_{H1}	Δy_{H1}	Δz_{H1}	Δx_{H2}	Δy_{H2}	Δz_{H2}
q_1	0.00547	-0.00554	0.09994	0.35209	0.31586	-0.49586	-0.38280	-0.28470	-0.49588
q_2	0.00550	-0.00557	0.00080	-0.17315	-0.20960	0.41467	0.14224	0.24096	0.41464
	Δx_{H3}	Δy_{H3}	Δz_{H3}	Δx_{H4}	Δy_{H4}	Δz_{H4}			
q_1	-0.05665	0.12396	-0.09771	0.02220	-0.08911	-0.10147			
q_2	-0.17478	0.24251	-0.41752	0.14011	-0.20744	-0.42131			

The coordinate q_1 points to the C_{2v} minimum of the GS cation while the coordinate q_2 points to the D_{2d} minimum. In addition, the Cartesian displacements Δ_i include distortions that allow spanning the NAC's seams between the three lowest states. On the grid, the point closest to a C_{2v} minimum on the ground state is at q_1 = -1.4 and q_2 = 0. It has a root mean square deviation (RMSD) of 0.0418 Bohr compared to the C_{2v} geometry. Strictly speaking, if there was no distortion and all the grid points were of C_{2v} symmetry, a second C_{2v} minimum should be present on the grid. However, maintaining the C_{2v} geometry for all grid points leads to zero non adiabatic coupling by symmetry. The other minimum on the grid corresponds to more

distorted C_{2v} geometry with a RMSD of 0.1384 Bohr with respect to C_{2v}, that is actually closer to a C_s symmetry. It is located at q_1=1.08 and q_2=1.26 and 0.1583 eV above the C_{2v} minimum on the grid. The D_{2d} minimum on the grid is localized at q_1= 0 and q_2 =-1.12 at a relative energy of 0.165 eV compared to the minimum C_{2v} on the grid. The RMSD from a D_{2d} geometry is 0.0321 Bohr. On the GS, the gradients from the T_d point on the grid in the directions of these three minima are nearly identical. The D1 PES on the grid exhibits three minima, localized close to the GS/D1 seams. There is a single well localized around T_d for D2 PES. Isocontours of the 3 PES are plotted in Figure S1.

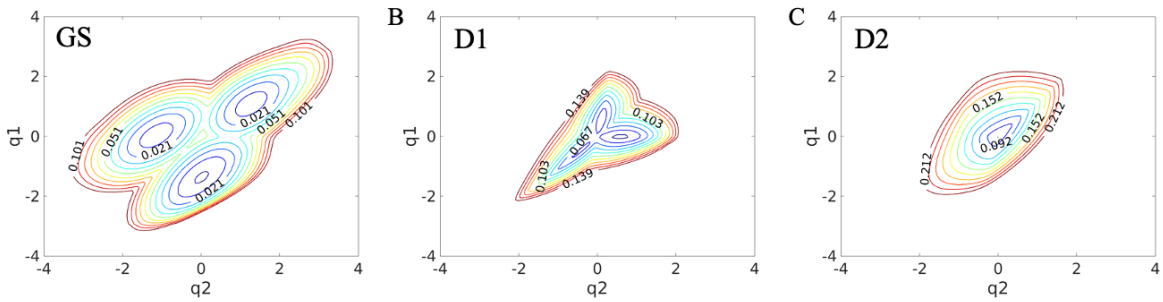

Figure S1: Isocontours of the PES of the cation computed at the SA-3-(9,8) /6-31G++(2df,2pd). A: Ground state. Isocontour spacing: 0.01 eV B. First excited state D1. Isocontour spacing: 0.009 eV. C. Second excited state D2. Isocontour spacing: 0.015 eV.

The size of the grid is defined to avoid reflections of the wave packet on the edges for the time range investigated . The grid extends from -5.8 to + 5.8 by step of 0.08 for q_1 and from -7.98 to 4.83 with a step 0.07 for q_2, which leads to 26864 grid points per electronic state. The FC region is defined by the ground vibrational state of the neutral at its equilibrium geometry. The D_{2d} and C_{2v} minima are located on the edges of the FC region which is centered on the Td geometry and comprises 1886 grid points. There is also C_{3v} minimum on the GS PES whose geometry falls outside the grid but whose computed energy and geometry are in agreement with ref. [1]. The decomposition of the two coordinates on the normal modes of the T_d, C_{2v} and

D_{2d} geometries of the GS of the cation is given in Tables S2 to S4. The position of the center of mass is conserved for all the geometries sampled by the grid. The Cartesian coordinates of the equilibrium geometries of the Td neutral ground electronic state and of the C_{2v} and D_{2d} minima of the ground state of the cation are given in Tables S5 to S7.

Table S2 : Decomposition of the two coordinates q_1 and q_2 in the normal modes of the Td of the GS neutral.

	$T_{2\text{-}b1}$	$T_{2\text{-}b1}$	$T_{2\text{-}b1}$	E_1	E_2	A_1	$T_{2\text{-}s1}$	$T_{2\text{-}s1}$	$T_{2\text{-}s1}$
q_1	-0.06209	0.12545	0.18221	0.17533	-0.51592	0.07245	-0.12389	-0.07338	-0.02498
q_2	-0.02390	-0.02341	0.00058	-0.05646	-0.99648	0.03965	0.01121	-0.01768	-0.02087

Table S3 : Decomposition of the two coordinates q_1 and q_2 in the normal modes of the C_{2v} minimum of the GS cation.

	A_2	$A_{1\text{-}1}$	$B_{2\text{-}1}$	$B_{1\text{-}1}$	$A_{1\text{-}2}$	$B_{2\text{-}2}$	$A_{1\text{-}3}$	$A_{1\text{-}4}$	$B_{1\text{-}2}$
q_1	0.38736	-0.15184	0.03143	-0.01828	-0.01556	-0.00512	-0.79214	0.09907	-0.02358
q_2	-0.34661	-0.13486	0.03163	-0.01839	-0.67273	-0.00051	0.64400	0.00654	-0.01224

Table S4 : Decomposition of the two coordinates q_1 and q_2 in the normal modes of the D_{2d} minimum of the GS cation.

	$E_{1\text{-}1}$	$E_{1\text{-}2}$	$B_{2\text{-}1}$	$A_{1\text{-}1}$	$B_{1\text{-}1}$	$B_{2\text{-}2}$	$A_{1\text{-}2}$	$E_{2\text{-}1}$	$E_{2\text{-}2}$
q_1	-0.02446	0.02775	0.68856	-0.45592	0.47398	0.13515	0.13121	-0.01927	0.01561
q_2	-0.02462	0.02773	0.02209	0.91015	0.06728	-0.06573	-0.11738	-0.01939	0.01571

Table S5: Cartesian coordinates of the equilibrium Td geometry of the neutral ground state computed at the CASSCF (10,8) /6-31G++(2df,2pd) in the laboratory frame defined in Figure 1A(in Bohr). The computed vertical IP is 13.61 eV. The T_d geometry is 1.81 eV above the C_{2v} minimum.

	X	Y	Z
C	0.0000	0.0000	0.0000
H1	1.2046	1.2046	1.2046
H2	-1.2046	-1.2046	1.2046
H3	1.2046	-1.2046	-1.2046
H4	-1.2046	1.2046	-1.2046

Table S6: Cartesian coordinates of the equilibrium C_{2v} geometry on the GS of the cation (global minimum) computed at the SA-3-CASSCF (9,8) /6-31G++(2df,2pd) in the laboratory frame defined in Figure 1A(in Bohr).

	X	Y	Z

C	0.0000	0.0000	-0.1494
H1	0.7033	0.7033	1.9477
H2	-0.7033	-0.7033	1.9477
H3	1.3166	-1.3166	-1.0578
H4	-1.3166	1.3166	-1.0578

Table S7: Cartesian coordinates of the equilibrium D_{2d} geometry on the GS of the cation computed at the SA-3-CASSCF (9,8) /6-31G++(2df,2pd) in the laboratory frame defined in Figure 1A(in Bohr). This local minimum is 0.2837 eV above the C_{2v} global minimum

	X	Y	Z
C	0.0000	0.0000	0.0000
H1	-1.4310	1.4310	0.7149
H2	1.4310	-1.4310	0.7149
H3	1.4310	1.4310	-0.7149
H4	-1.4310	-1.4310	-0.7149

Vibronic Hamiltonian on the grid

We use atomic units throughout. In the $\left(q_1,q_2\right)$ coordinates, the kinetic energy operator takes the form :

$$\hat{T} = -\frac{1}{2}\left(\frac{1}{\mu_1}\frac{\hat{\partial}^2}{\partial q_1^2} + \frac{1}{\mu_2}\frac{\hat{\partial}^2}{\partial q_2^2} + \frac{2}{\mu_{12}}\frac{\hat{\partial}^2}{\partial q_1 \partial q_2}\right)$$
$$\mu_1^{-1} = \sum_i \frac{1}{m_i}\sum_\alpha^3 a_{i\alpha}^2, \quad \mu_2^{-1} = \sum_i \frac{1}{m_i}\sum_\alpha^3 b_{i\alpha}^2, \quad \mu_{12}^{-1} = \sum_i \frac{1}{m_i}\sum_\alpha^3 b_{i\alpha}a_{i\alpha} \tag{3}$$

with m_i being the mass of C and H respectively.

The Hamiltonian includes the non adiabatic coupling between the three lowest electronic states of the cation. The basis functions are the product of the adiabatic electronic wave function of state i, $\left|\Psi_{ig}^{elec}\right\rangle$, computed at the grid point g which corresponds to a value of q_1 and q_2 and a product of orthonormal window functions $\theta_g = \theta\left(q_{1g}\right)\theta\left(q_{2g}\right)$ centered at each grid point. In short notation we denote the full wave function at each grid point $\left|ig\right\rangle$. After integration on the electronic coordinates, the matrix elements of the Hamiltonian between two basis wave functions $\left|ig\right\rangle$ and $\left|jg'\right\rangle$ take the form:

$$\mathbf{H}_{ig,jg'}(t) = -\frac{1}{2}\mathbf{T}_{ig,jg'}\delta_{ij} + \mathbf{V}_{ig,jg'}\delta_{ij}\delta_{gg'} + \left(\frac{1}{i}\tau_{ig,jg}\delta_{gg'}\right).\mathbf{p}_{jgg'} \quad (4)$$

where *i* and *j* stand for the electronic state index and *g* and *g'* for the indices of grid points. $\mathbf{T}_{ig,jg'}$ are the matrix elements of the kinetic energy operator defined in Eq.(3), they are diagonal in the electronic state index but off diagonal in the grid point index. $\mathbf{V}_{ig,jg'}$ are the matrix elements of the potential energy, diagonal in both the electronic and grid indexes.

The non adiabatic coupling (NAC) matrix elements are computed at each grid point, using the quantum chemistry program MOLPRO.[2] $\boldsymbol{\tau}_{ig,jg}$ is the NAC vector expressed in the coordinates (q_1, q_2), see Figure S4 for a heatmap of the two components on the grid. It is diagonal in the grid point index, *g*, but off diagonal in the electronic state index. We neglect in Eq. (4) the second derivative matrix elements with respect to the nuclear coordinate of the electronic wave function. $\mathbf{p}_{jgg'}$ is the matrix of the momentum operator on state *j* with $\hat{p}_1 = -i(\partial/\partial q_1)$ and $\hat{p}_2 = -i(\partial/\partial q_2)$.

The time-dependent Schrödinger equation

$$i\frac{d\mathbf{c}}{dt} = \mathbf{H}\mathbf{c} \quad (5)$$

is integrated numerically for a vector of amplitudes, **c**, of $L=N$g x 3 =80592 complex components. The action of the non local kinetic energy is computed using a finite difference scheme with $O(h^4)$ error.[3, 4] We use a $O(h^6)$ for the momentum operator to retain a good numerical precision in the integration of the terms due to the NAC coupling.

The first-order derivatives are computed at order 6 as [5].

$$\frac{dc_{u,v}}{du} = \frac{1}{60du}\left(-c_{u-3,v} + 9c_{u-2,v} - 45c_{u-1,v} + 45c_{u+1,v} - 9c_{u+2,v} + c_{u+3,v}\right), \quad u, v = q_1, q_2 \quad (6)$$

where *u* and *v* represents the q_1 and q_2 coordinates corresponding to a grid point *g*. The second order derivatives are given by[5]:

$$\frac{d^2 c_{u,v}}{du^2} = \frac{1}{12du^2}\left(-c_{u-2,v} + 16c_{u-1,v} - 30c_{u,v} + 16c_{u+1,v} - c_{u+2,v}\right) \quad (7)$$

and the cross derivatives between the two internal coordinates *v* and *u*:

$$\frac{dc_{u,v}}{dvdu} = \frac{1}{2dvdu}\left(-c_{u,v+1} - c_{u,v-1} - c_{u+1,v} - c_{u-1,v} + c_{u-1,v-1} + c_{u+1,v+1} + 2c_{u,v}\right) \quad (8)$$

The amplitudes $c_{ig}\left(t\right)$ are propagated using Eq. (5) using a time step of 0.01 a.u. of time and a 4th order Runge-Kutta scheme for the time integration which allows to keep the norm up to 10^{-8} for the time range of 50 fs investigated.

Initial density matrix of the ensemble.

We draw an ensemble, a mixture of 8000 initial states, with random orientations, $\hat{\mathbf{e}}$, of the electric field with respect to the molecular frame. For each orientation, $\hat{\mathbf{e}}$, and each carrier frequency, $h\nu_9$ or $h\nu_{11}$, of the ionizing pulse, we define a vector, $\mathbf{c}_m$, of complex amplitudes, c_{ig}^m, on the grid points $\left(q_1, q_2\right)$ for each electronic state *i*, i =1, 2, 3 :

$$c_{ig}^m = c_{GS,g}^{neut}\sqrt{\rho\left(g,\varepsilon\right)}\hat{\mathbf{e}}_m.\mathbf{d}_{ig}^{\varepsilon} \quad (9)$$

where *m* is the index for the initial conditions, $\hat{\mathbf{e}}_m$, for a given value of the carrier frequency of the pulse and *ig* is the electronic state-grid index. $\rho\left(g,\varepsilon\right) = \sqrt{\varepsilon}$ is the density of states computed at grid point *g* for an ionization for electronic state *i*. The kinetic energy of the photoelectron at each grid point g for a given electronic state, *i,* is given by $\varepsilon = h\nu - \left(V_{ig}^{cat} - V_{GSg}^{neut}\right)$ for a given carrier frequency, $h\nu$, of the XUV pulse.

The $\mathbf{d}_{ig}^{\varepsilon}$ are the photoionization matrix elements from the GS neutral to the three electronic states of the cation at each grid point integrated over the solid angle $\hat{\Omega}$:

$$\mathbf{d}_{ig}^{\varepsilon} = \sqrt{2}\int d\hat{\Omega}\int d\mathbf{r}\,\phi_{GS-ig}^{D}(\mathbf{r})\,\mathbf{r}\,\phi_{\varepsilon,\hat{\Omega}}^{elec\perp}(\mathbf{r}) \qquad (10)$$

The $\mathbf{d}_{ig}^{\varepsilon}$'s are computed within the sudden ionization approximation for each grid point in the FC region as described in ref. [6]. $\phi_{GS-ig}^{D}(\mathbf{r})$ is the Dyson orbital between the GS of the neutral and the electronic state *i* of the cation computed at grid point *g* at the CASSCF (10,8) and SA3-CASSCF (9,8) levels with the atomic basis set /6-31G++(2df,2pd) respectively. The photoelectron wave functions, $\phi_{\varepsilon,\hat{\Omega}}^{elec\perp}(\mathbf{r})$, are orthogonalized plane waves with $\varepsilon = k^2/2$, for the wave vector **k**. The photoelectron continuum is discretized in 256 *k* values. For each *k* value, an ensemble of 512 values of solid angles are sampled uniformly on the unit sphere.

The norms of the vectors $|\mathbf{c}_m|^2 = \sum_{ig} \left|c_{ig}^{m}\right|^2$, are the ionization yields normalized to the strength of the electrical field, $P_{h\nu,\hat{\mathbf{e}}}$, of the neutral in the direction $\hat{\mathbf{e}}$ for a carrier frequency $h\nu$, shown in Figure 2 of the main text for CH_4^+ and in Figure S2 for CD_4^+. Each vector $\mathbf{c}_m$ defines a pure state and the corresponding *L* by *L* density matrix, $\rho_m(0)$, takes the form:

$$\rho_m(0) = \mathbf{c}_m\mathbf{c}_m^{\dagger} \qquad (11)$$

The ensemble density matrix, $\rho_{ens}(0)$ at time *t* = 0, is the sum of the matrices $\rho_m(0)$:

$$\rho_{ens}(0) = \sum_{m=1}^{M} \rho_m(0) = \sum_{m=1}^{M} \mathbf{c}_m\mathbf{c}_m^{\dagger} \qquad (12)$$

where *M* is the number of orientations of the electric field. Both the density matrix, $\rho_m(0)$, Eq. (11), of a particular orientation, $\hat{\mathbf{e}}_m$, of the electric field in the laboratory frame and the ensemble density matrix, $\rho_{ens}(0)$, Eq. (12), can be written as a quadratic form. Each matrix $\rho_m(0)$ is a pure case of rank 1. For $\rho_{ens}(0)$ one can define a rectangular matrix **A**, of dimensions *L* x *M*, made of the *M* vectors $\mathbf{c}_m$, so that it takes the form

$$\rho_{ens}(0) = \mathbf{A}\mathbf{A}^{\dagger} \tag{13}$$

For the case studied here, we have that M, the number of random orientations of the electric field is much smaller than L the number of grid points in 2D multiplied by the number of electronic states. We expect that $M << L$ will typically be the case when averaging over orientations in the case of a multistate quantum dynamics on a multidimensional grid. One can then apply a singular value decomposition (SVD) on the matrix **A** directly:

$$\mathbf{A} = \mathbf{S}\Sigma\mathbf{V}^{\dagger} \tag{14}$$

where **S** is a L x M matrix of the complex left eigenvectors of **A**, Σ the M x M diagonal matrix of its eigenvalues and the columns of M x M matrix **V** are the complex right eigenvectors. One can show that $\rho_{ens}(0)$ has at most M non zero eigenvalues that are given by the squares of the M eigenvalues of the matrix **A**. The eigenvectors of the $\rho_{ens}(0)$ that correspond to its non zero eigenvalues are the M left eigenvectors of the **A** matrix given by the matrix **S** in Eq. (14) above. The SVD decomposition of the L by M **A** therefore provides a computationally less demanding route than diagonalizing the Hermitian L x L $\rho_{ens}(0)$ density matrix, since we have $M << L$.

In the case of a random orientation of the electric field in the laboratory frame, one can show analytically that there are only three non zero eigenvalues of the matrix **A**, which leads to a very large saving of computer time for computing the time evolution of the ensemble.

From Eqs. (9) and (10), one can define a transition dipole vector at each grid point weighted by the amplitude of the neutral ground state, $c_{GS,g}^{neut}$:

$$\bar{\mathbf{d}}_{ig} = c_{GS,g}^{neut}\sqrt{\rho(\varepsilon)}\mathbf{d}_{ig}^{\varepsilon} \tag{15}$$

so that we can rewrite the amplitude of the initial state on the grid (Eq. (9)) as

$$c_{ig}^{m} = \hat{\mathbf{e}}_{m}^{T}.\bar{\mathbf{d}}_{ig} \tag{16}$$

Using this notation, one matrix element *ig,jg'* of L x L $\rho_{ens}(0)$ in Eq. (12) takes the form

$$\rho_{ens}^{ig,jg'} = \sum_m \left(\hat{\mathbf{e}}_m^T.\overline{\mathbf{d}}_{ig}\right)^\dagger \left(\hat{\mathbf{e}}_m^T.\overline{\mathbf{d}}_{jg'}\right) = \sum_m \left(\overline{\mathbf{d}}_{ig}^\dagger.\hat{\mathbf{e}}_m\right)\left(\hat{\mathbf{e}}_m^T.\overline{\mathbf{d}}_{jg'}\right)$$
$$= \overline{\mathbf{d}}_{ig}^\dagger \left(\sum_m \hat{\mathbf{e}}_m \hat{\mathbf{e}}_m^T\right)\overline{\mathbf{d}}_{jg'} \qquad (17)$$

where the normalized vectors $\hat{\mathbf{e}}_m$ have each 3 Cartesian components : $\hat{\mathbf{e}}_m = \begin{pmatrix} X_m & Y_m & Z_m \end{pmatrix}^T$. The matrix $\sum_{m=1}^{M} \hat{\mathbf{e}}_m.\hat{\mathbf{e}}_m^T$ is a 3x3 matrix which for random orientations of the vectors $\hat{\mathbf{e}}_m$ is diagonal and is a multiple of the unit matrix by a constant that depends on the number of samplings, *M*. It can therefore be factorized in front of the row vector $\overline{\mathbf{d}}_{ig}^\dagger$ in Eq. (17). Since each column vector $\overline{\mathbf{d}}_{ig} = \begin{pmatrix} \overline{d}_{ig}^X & \overline{d}_{ig}^Y & \overline{d}_{ig}^Z \end{pmatrix}^T$ has three Cartesian components, the expression of the full matrix $\rho_{ens}(0)$ given in Eq. (12) and Eq. (13) becomes is a *L* x *L* matrix that is the product of the *L*x3 matrix $\overline{\mathbf{d}}^\dagger$ and the 3x*L* matrix $\overline{\mathbf{d}}$. So in case of a random orientation of the electric field with respect to the molecular frame, the quadratic form of $\rho_{ens}(0)$ in Eq. (13) takes a simpler form where the matrix **A** is replaced by the matrix $\overline{\mathbf{d}}$:

$$\rho_{ens}(0) = \overline{\mathbf{d}}^\dagger\overline{\mathbf{d}} = \begin{pmatrix} \overline{d}_1^X & \overline{d}_1^Y & \overline{d}_1^Z \\ \vdots & \vdots & \vdots \\ \\ \\ \overline{d}_L^X & \overline{d}_L^Y & \overline{d}_L^Z \end{pmatrix} \begin{pmatrix} \overline{d}_1^X & \cdots & \overline{d}_L^X \\ \overline{d}_1^Y & \cdots & \overline{d}_L^Y \\ \overline{d}_1^Z & \cdots & \overline{d}_L^Z \end{pmatrix}^* \qquad (18)$$

$\rho_{ens}(0)$ is therefore of rank 3 and its spectral representation takes the form :

$$\rho_{ens}(0) = \sum_{r=1}^{3} \omega_r^2 \mathbf{s}_r \mathbf{s}_r^\dagger \qquad (19)$$

where the eigenvectors $\mathbf{s}_r$ are complex and orthonormal. The eigenvectors of $\rho_{ens}(0)$ that correspond to a non zero eigenvalue are given by the left eigenvectors of the SVD decomposition of the matrix $\bar{\mathbf{d}}$ in Eq. (18) :

$$\bar{\mathbf{d}} = \mathbf{S_d}\Sigma_\mathbf{d}\mathbf{V}_\mathbf{d}^\dagger \qquad (20)$$

$\mathbf{S_d}$ is the L x 3 matrix of the left eigenvectors of $\bar{\mathbf{d}}$, the three $\mathbf{s}_r$ eigenvectors of $\rho_{ens}(0)$. $\Sigma_\mathbf{d}$ is the 3 x 3 matrix of the eigenvalues and $\mathbf{V}_\mathbf{d}^\dagger$ is the 3x3 matrix of the right eigenvectors. The eigenvalues of $\rho_{ens}(0)$ are given by the squares of the eigenvalues of $\bar{\mathbf{d}}$. To compute the time evolution of the density matrix of the ensemble, it is therefore strictly equivalent to either propagate the M=8000 $\mathbf{c}_m$ vectors or to propagate the three $\mathbf{s}_r$ vectors using the time dependent Schrödinger equation (Eq. (5)). This is because the time evolution of $\rho_{ens}(0)$ is unitary and dictated by the Hamiltonian (Eq. (4)). Diagonalizing the $\bar{\mathbf{d}}$ matrix by SVD and propagating its left eigenstates therefore provides a considerable saving of computer times and allows running quantum dynamics for an accurate sampling of the random initial orientations. We checked numerically that it was indeed the case. In general, even if the orientation of the orientations of the electric field in the laboratory frame are not random, diagonalizing the A matrix of Eq. (14) provides a saving of computer time as long as $M << L$ because $\rho_{ens}(0)$ is rank deficient and can have at most M non zero eigenvalues.

The three eigenvalues of $\bar{\mathbf{d}}$ are not equal, which can be understood because the cartesian components of the photoionization matrix elements $\mathbf{d}_{ig}^{\varepsilon}$ are no equal and depend on the grid point g and on the electronic state i. For a given carrier frequency of the XUV ionizing pulse, the traces of $\bar{\mathbf{d}}$ reported in Table S4 are almost identical for CH_4^+ and CD_4^+. The eigenvalues of $\bar{\mathbf{d}}$ and its traces are reported in Table S4, as well as the trace of $\rho_{ens}(0)$ for the four computations. Each $\mathbf{s_r}$ vector has amplitudes on the three electronic states. The three right eigenvectors are localized along the X, Y, and Z directions.

Table S8 : Trace of the matrix $\rho_{ens}(0)$ and the three eigenvalues normalized to the trace for the four computations.

	$h\nu_9$		$h\nu_{11}$	
	CH_4^+	CD_4^+	CH_4^+	CD_4^+
Trace	94.3975	94.5496	109.1024	108.6559
ω_1	0.5442	0.5360	0.8380	0.8420
ω_2	0.3253	0.3282	0.1150	0.1152
ω_3	0.1343	0.1358	0.0469	0.0427

Supplemental figures

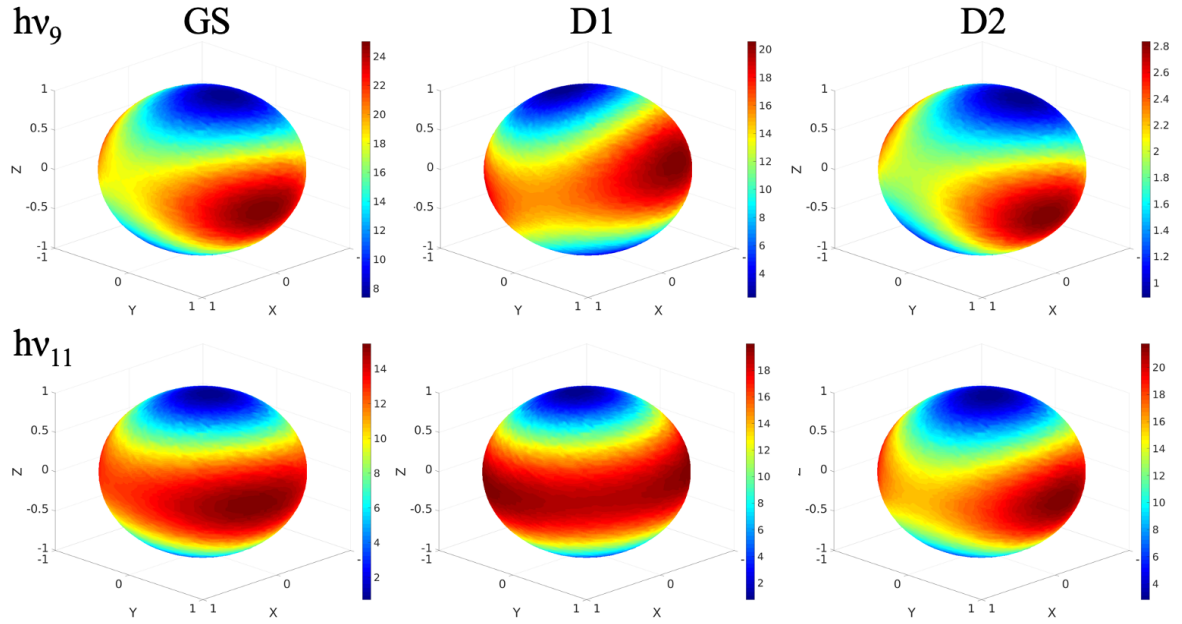

Figure S2 : Heatmaps of angularly resolved photoionization yields plotted separately for each electronic state ($\sum_g \left|c_{ig}^m\right|^2$ with i = GS, D1 and D2) computed for CD_4^+ and two carrier frequencies of the ionization XUV attopulse ($h\nu_9$ = 13.95 eV and $h\nu_{11}$= 17.05 eV). The heatmaps are computed by drawing 8000 $\mathbf{c}_m$ vectors with random orientations $\hat{\mathbf{e}}$ of the electric field. Note how for the D2 state, the yield is very small for the 9th harmonic while it is comparable to the lowest states for the 11th one.

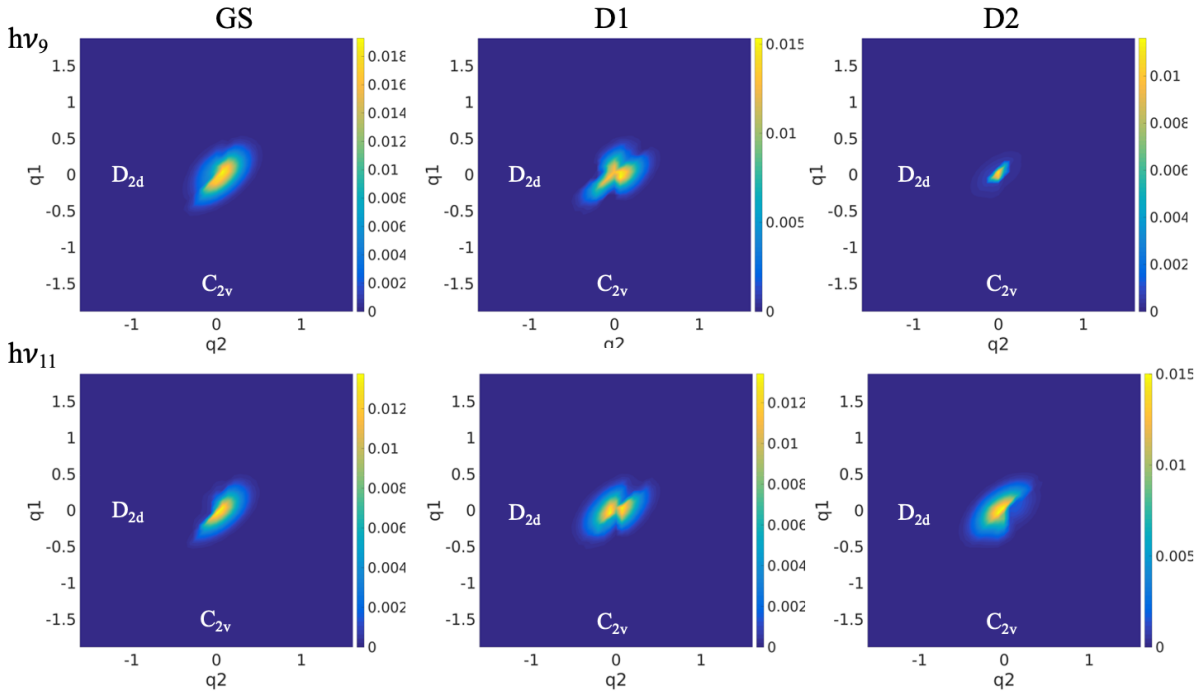

Figure S3 : Heatmaps of the population on each grid point, $\left[\rho_{ens}(0)\right]_{ig,ig}$ on each electronic state i = GS (left), D1 (middle) and D2 (right), computed for CD_4^+ for the $h\nu_9$ (top row) and $h\nu_{11}$ (bottom row) pulses.

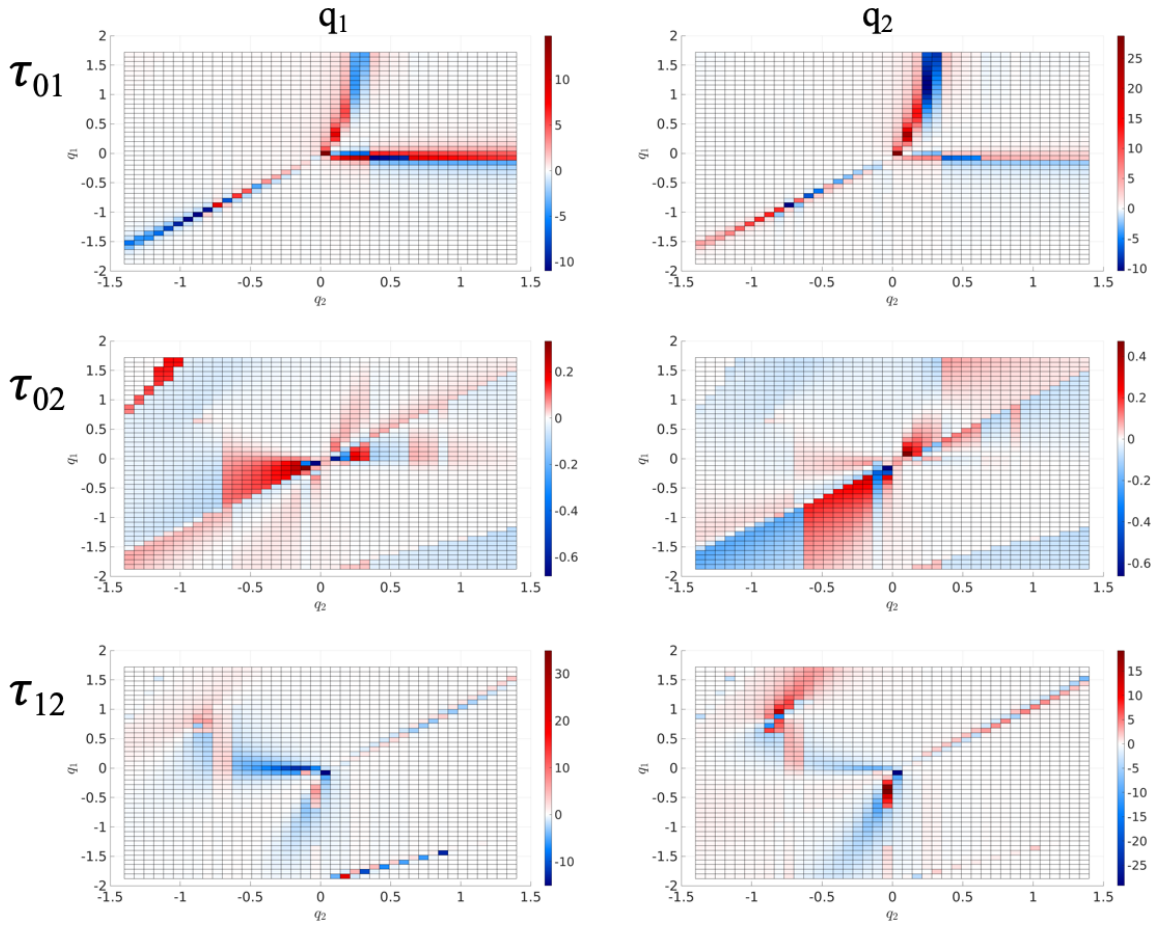

Figure S4. Heatmaps of the components of the NAC vector along the coordinates q_1 and q_2 on the grid as indicated.

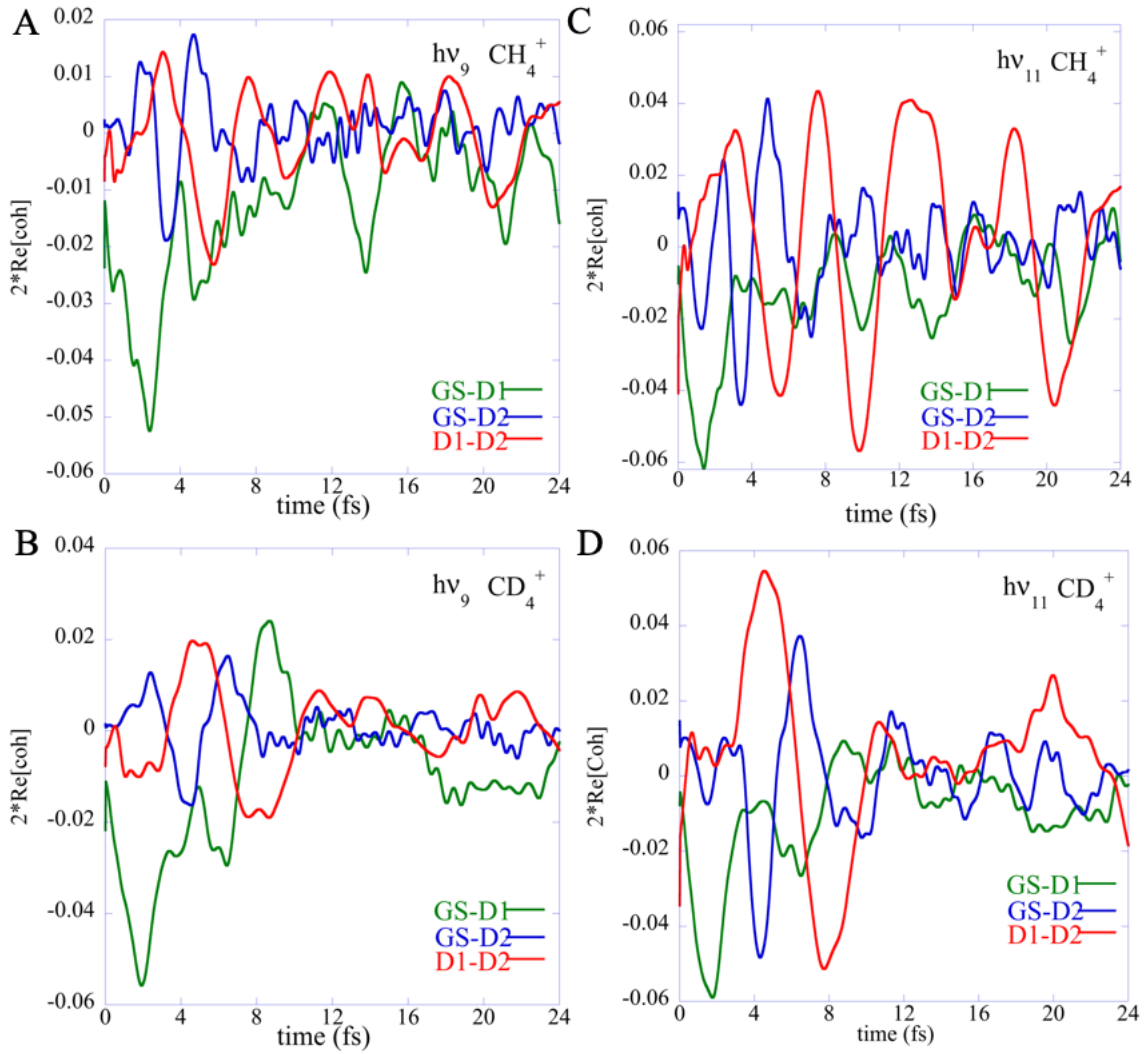

Figure S5: Time evolution of the three electronic coherences, integrated over the full grid $2\,\mathrm{Re}\left[\sum_{g}\rho_{ig,jg}(t)\right]$. The GS-D1 (i=GS, j=S1) is plotted in green, the GS-D2 (i=GS, j=S2) is plotted in blue and the D1-D2 coherence (i=S1, j=S2) is plotted in red. Panel A : Ionization by the $h\nu_9$ pulse, CH_4^+, B : Ionization by the $h\nu_9$ pulse, CD_4^+, C :Ionization by the $h\nu_{11}$ pulse, CH_4^+, D : Ionization by the $h\nu_{11}$ pulse, CD_4^+.

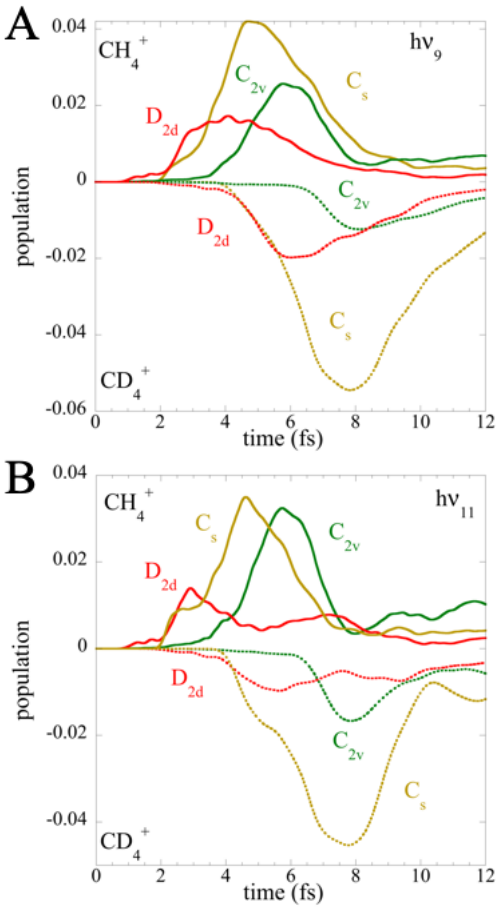

Figure S6: Populations in a region of 25 grid points localized around the D_{2d} (red), C_{2v} (green) and C_s (bronze) minima on the GS computed for CH_4^+ and CD_4^+ with the $h\nu_9$ pulse (panel A) and the $h\nu_{11}$ pulse (panel B). The RMSD deviation of the 25 point region from the D_{2d} geometry is 0.0504 1 Bohr (similar to that computed for the minimum grid point shown in figure 4 C and D), for the C_{2v} region, the RMSD with respect to the C_{2v} geometry is 0.0571, and for the C_s 25 point region, the RMSD with respect to a C_{2v} geometry is 0.1438 Bohr. One clearly see that the onset of the rise of the population in the D_{2d} region precedes that in the C_s region, with the onset of the rise in the C_{2v} occurring later.

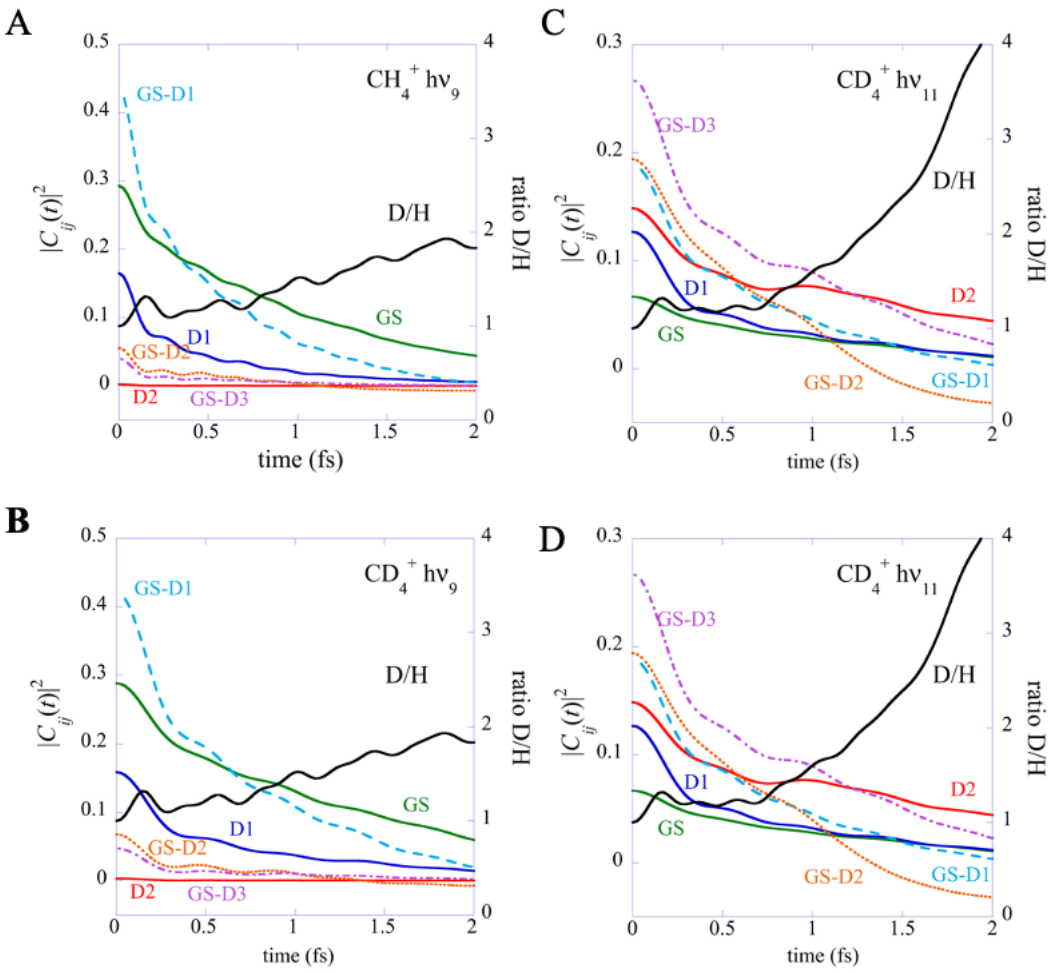

Figure S7: The contributions of the electronic coherences to the square moduli of the autocorrelations for the four dynamical simulations as indicated, panel A : CH_4^+, $h\nu_9$, B: CD_4^+, $h\nu_9$, C: CH_4^+, $h\nu_{11}$ and D: CD_4^+, $h\nu_{11}$. The ratio of the autocorrelation functions $|C(t)_D|^2/|C(t)_H|^2$ is plotted in black. Note how the difference in the decay of the GS-D2 term and to a smaller extent that of the GS-D1 term coincides with the onset of a large isotope effect in the $h\nu_{11}$ dynamics.

$$\left|C(t)\right|^2 = \sum_{i=1}^{3} \sum_{gg'} c_{ig}^{*}(0) c_{ig}(t) c_{ig'}(0) c_{ig'}^{*}(t) + \sum_{i,j\neq i}^{3} \sum_{gg'} c_{ig}^{*}(0) c_{ig}(t) c_{jg'}(0) c_{jg'}^{*}(t)$$

, i = GS, D1, D2.

References

1. R. F. Frey and E. R. Davidson, *J. Chem. Phys.*, 1988, **88**, 1775-1785.
2. H.-J. Werner, P. J. Knowles, G. Knizia, F. R. Manby and M. Schütz, *Wiley Interdisciplinary Reviews: Computational Molecular Science*, 2012, **2**, 242-253.

3. S. A. Jayantha, K. G. Komarova, S. v. d. Wildenberg, F. Remacle and R. D. Levine, in *Attosecond Molecular Dynamics*, eds. M. J. J. Vrakking and F. Lepine, Royal Society of Chemistry, Cambridge, 2018, vol. 13, pp. 308-347.
4. K. G. Komarova, F. Remacle and R. D. Levine, *Mol. Phys.*, 2018, **116**, 2524-2532.
5. M. Abramovitz and I. Stegun, *A Handbook of Mathematical Functions*, Dover, New York, 1972.
6. S. van den Wildenberg, B. Mignolet, R. D. Levine and F. Remacle, *J. Chem. Phys.*, 2019, **151**, 134310.